NMR Structural Study of TcUBP1, a Single RRM Domain Protein from *Trypanosoma cruzi*: Contribution of a β Hairpin to RNA Binding[†,‡]

Laurent Volpon,[§,||] Iván D'Orso,[⊥,#] Christopher R. Young,[§] Alberto C. Frasch,[⊥] and Kalle Gehring*[,§]

Department of Biochemistry, McGill University, McIntyre Medical Science Building, 3655 Promenade Sir-William-Osler, Montreal, Québec, H3G 1Y6, Canada, and Instituto de Investigaciones Biotecnológicas-UNSAM Av Gral Paz 5445, 1650 INTI, Edificio 24, San Martin, Buenos Aires, Argentina

Received December 6, 2004; Revised Manuscript Received January 11, 2005

ABSTRACT: TcUBP1 is a trypanosome cytoplasmic RNA-binding protein containing a single, conserved RNA-recognition motif (RRM) domain involved in selective destabilization of U-rich mRNAs such as the *Trypanosoma cruzi* small mucin gene family mRNA, *TcSMUG*. TcUBP1 binds specific transcripts *in vivo* and co-localizes in the perinuclear part of the cell with components of the mRNA-stability determinant pathway such as poly(A)-binding protein 1 (PABP1) and TcUBP2, a closely related RRM-containing protein. In TcUBP proteins, the RRM domain is flanked by N-terminal Gln-rich and C-terminal Gly-Gln-rich extensions, which are involved in protein−protein interactions. In this work, we determined the solution structure of the TcUBP1 RRM domain by nuclear magnetic resonance (NMR) spectroscopy. The domain has a characteristic $\beta\alpha\beta\beta\alpha\beta$ fold, consisting of a β sheet composed of four antiparallel β strands and two α helices packed against one face of the β sheet. A unique aspect of TcUBP1 is the participation of a β hairpin ($\beta4-\beta5$) in the β sheet, resulting in an enlarged RNA-binding surface. Detailed analysis of the TcUBP1 interaction with a short single-stranded RNA derived from the 3′ UTR of *TcSMUG* was carried out by titration experiments using both NMR spectroscopy and isothermal titration calorimetry. This analysis revealed that amino acids located within the β hairpin ($\beta4-\beta5$) contribute to complex formation. This enlarged protein−RNA interface could compensate for the lack of additional RNA-binding domains in TcUBP1, as observed in many other RRM-containing proteins. The structure of TcUBP1 reveals new aspects of single RRM−RNA interactions and insight into how N- and C-terminal extensions can contribute to RNA binding.

Trypanosomes are widespread protozoan microorganisms from the order Kinetoplastida, which cause important health problems in millions of people. The causative agent of Chagas disease or American trypanosomiasis is the protozoan parasite *Trypanosoma cruzi* (*1*). In this unicellular organism, transcription is not the major point of control of gene expression. In fact, protein expression is unique in that it is not regulated through transcription initiation but via post-transcriptional regulatory mechanisms, including trans-splicing coupled with polyadenylation (*2*) and modifications of mRNA half-life (*3*, *4*). In particular, post-transcriptional mechanisms mediated by RNA-binding proteins (RBPs)[1] are of key importance in the expression of life-cycle-dependent antigens and regulatory factors. The major group of RBPs in trypanosomes is the RNA-recognition motif (RRM) group [alternatively known as RBD (RNA-binding domain)] (*5*). In addition to this motif, zinc finger, SR-rich, RGG-box, and PUF-containing RBPs have been described. These ribonucleoprotein (RNP) complexes are involved in a compendium of processes in these organisms such as transcription, RNA processing, localization, and translation (reviewed in ref *5*).

A key element involved in mRNA stabilization/destabilization is the AU-rich element (ARE) located in the 3′ untranslated region (UTR) of short-lived mRNAs (*6*, *7*). This cis-acting degradation signal identified first in proto-oncogenes, lymphokines, and cytokines is divided into three classes depending on the copy number (class I and II) and/or the absence (class III) of the AUUUA motif. Many proteins that bind such motifs have been described biochemi-

[†] This work was supported by Grant AI060645-01 from the National Institutes of Health and an International Research Scholar grant from the Howard Hughes Medical Institute to A.C.F. and Grant MOP-14291 from the Canadian Institutes of Health Research to K.G. I.D. is a Research Fellow, and A.C.F. is a Researcher of the National Research Council (CONICET), Argentina.

[‡] PDB accession number 1U6F.

* To whom correspondence should be addressed. E-mail: kalle.gehring@mcgill.ca. Telephone: (514) 398-7287. Fax: (514) 847-0220.

[§] McGill University.

[||] Present address. Institut de Recherche en Immunovirologie et Cancérologie, Université de Montréal, 2900 Bld Edouard Montpetit, Montréal, Québec, H3T 1J4, Canada.

[⊥] Instituto de Investigaciones Biotecnológicas.

[#] Present address. University of California−San Francisco, Department of Biochemistry and Biophysics, 600 16th Street, CA 94143-2280.

[1] Abbreviations: ARE, AU-rich element; HMQC, heteronuclear multiple-quantum correlation; hnRNP, heterogeneous nuclear ribonucleoprotein; HSQC, heteronuclear single-quantum correlation; NOESY, nuclear Overhauser effect spectroscopy; PABP, poly(A)-binding protein; RBD, RNA-binding domain; RBP, RNA-binding protein; RNP, ribonucleoprotein; RRM, RNA-recognition motif; *TcSMUG*, *Trypanosoma cruzi* small mucin gene family; Sxl, sex-lethal protein; TcUBP, *Trypanosoma cruzi* uridine-rich-binding protein; TOCSY, total correlation spectroscopy; UTR, untranslated regions.

10.1021/bi047450e CCC: $30.25
Published on Web 02/12/2005

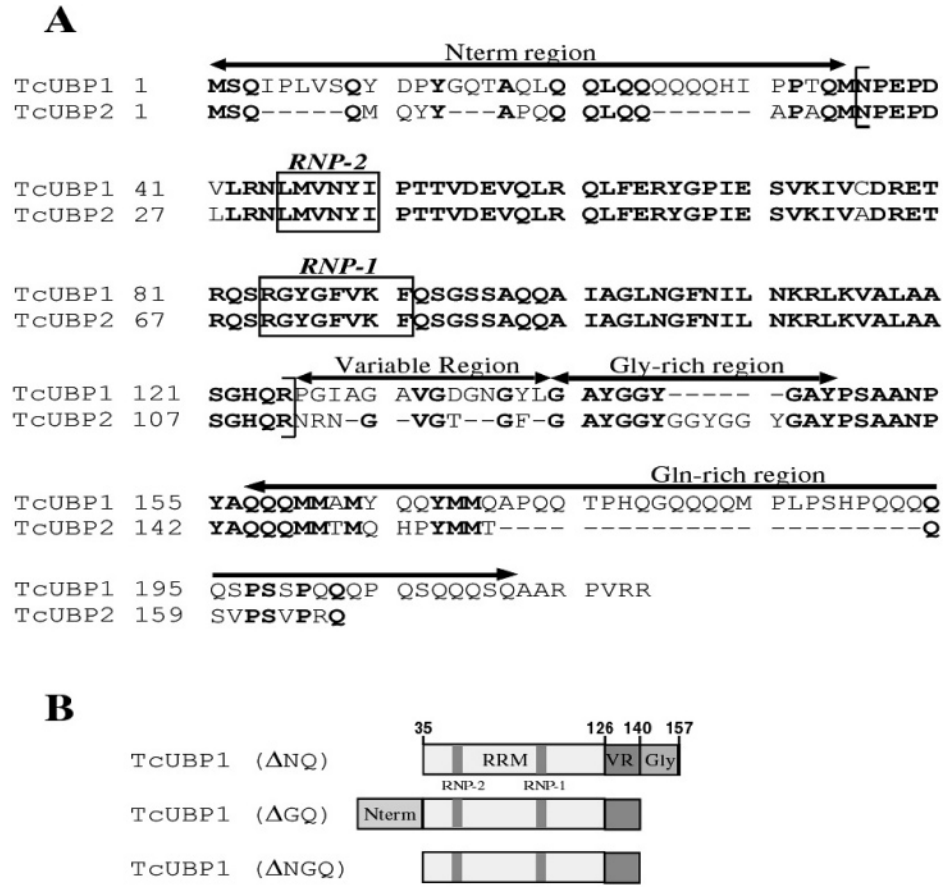

FIGURE 1: (A) Sequence alignment of TcUBP1 and TcUBP2. The different domains constituting the proteins are the N-terminal region (Nterm), the RRM (delimited by brackets) comprising the two RNP sequences, the variable region (VR), and the Gly- and Gln-rich regions. Identical residues between both proteins are shown in bold. (B) Scheme of TcUBP1 and the different TcUBP1 constructs used in this paper.

cally and structurally, of which the ELAV/Hu protein family (*8*−*11*), the human U1 small nuclear ribonucleoprotein A (*12*−*15*), and heterogeneous nuclear ribonucleoprotein (hnRNP) A1 and C (*16*, *17*) have been studied the most. In these RBPs, RRM domains, typically present in 1−3 copies, are an evolutionarily conserved domain of ~90 amino acids characterized by a $\beta\alpha\beta\beta\alpha\beta$ topology. It contains two signature sequences, RNP2 and RNP1, that form the central part of the β sheet and are involved in RNA binding (*18*, *19*).

In trypanosomes, one of the best studied RBPs is the uridine-rich-binding protein 1 (TcUBP1) from *Trypanosoma cruzi*, a single RRM domain protein containing a short Gln-rich N-terminal region and a Gly-Tyr and Gln-rich C-terminal region (Figure 1A) (*20*). TcUBP1 interacts with U-rich stretches, especially those containing guanosines or adenosines interspersed between tracts of 4 or 5 uridines (20). TcUBP1 was also shown to interact *in vivo* with 3′-UTR U-rich transcripts such as the mucin *TcSMUG* group, tssa and amastin (*21*). Interestingly, TcUBP1 interacts with *TcSMUG* only in a life-cycle-stage-dependent manner, and its overexpression produced the accelerated decay of mucin *TcSMUG* mRNA (*20*). Additionally, we described another single RRM-containing RBP named TcUBP2, which possesses a Gly-Tyr-rich C-terminal region extension. TcUBP1 and TcUBP2 have a common core structure and were predicted to fold into the three-dimensional structure characteristic of RRMs (*19*). The RRM domain is the most highly conserved region and responsible for RNA binding (*22*). The N- and C-terminal regions of both TcUBPs are more divergent and thought to be involved in recruiting different factors to RNP complexes (D'Orso et al., unpublished data). The TcUBP1 Gly-rich domain was shown to be involved in homo- and heterodimerization with TcUBP2 (*22*). TcUBP1 also interacts with poly(A)-binding protein 1 (PABP1) and inhibits its binding to *TcSMUG* mRNA. This consequently contributes to destabilization of the mRNA (*20*, *22*).

To obtain insight into how TcUBP1 interacts with its different partners to regulate mRNA stability, we determined the solution structure of TcUBP1 and analyzed by nuclear magnetic resonance (NMR) chemical-shift mapping its interactions with the GU-rich RNA element from one of its target mRNAs, *TcSMUG*. The study provides a structural framework for further biochemical studies of TcUBP1 function.

EXPERIMENTAL PROCEDURES

Preparation of NMR Samples. Different TcUBP1 recombinant protein deletions, termed ΔNQ, ΔGQ, and ΔNGQ, were prepared by PCR as previously described (*22*) (Figure 1B). The primers used for TcUBP1 protein deletions were as follows: NH_2-int-*Bam*HI (5′-CGGGATCCATGAACCCC-GAGCCCGATGTT-3′) and Gln-as-*Eco*RI (5′-CGAATTCT-TACGCGTACGGGTTCGCAGCG-3′) for TcUBP1 (ΔNQ), NH_2-*Bam*HI (5′-CGGGATCCATGAGCCAAATTCCGT-TGGTTTC-3′) and NES-as-*Eco*RI (5′-CGAATTCTTAGG-GGCGCTGGTGACCACTGGCC-3′) for TcUBP1 (ΔGQ), and NH_2-int-*Bam*HI and NES-as-*Eco*RI for TcUBP1 (ΔNGQ).

TcUBP1 (ΔGQ) was used for the determination of the NMR structure; TcUBP1 (ΔNQ) was used for the isothermal titration calorimetry (ITC) and NMR titrations with RNA; and TcUBP1 (ΔNGQ) was used additionally for the ITC titration. All fragments were cloned into a pGEX2T plasmid (Amersham) that expresses glutathione-*S*-transferase (GST) fusion proteins containing a thrombin protease site. The C terminus of TcUBP1 (ΔNQ) includes six extra amino acids (EFIVTD). Plasmids were transformed into *Escherichia coli* strain BL21 Gold/DE3 (Stratagene). Unlabeled or uniformly isotope-labeled protein was obtained by growing bacteria at 37 °C in Luria−Bertani (LB) or M9 minimal medium containing 0.5 g of ^{15}N-NH_4Cl and/or 2 g of $^{13}C_6$-glucose (Cambridge Isotope Laboratory) per liter of media and 100 μg/mL of ampicilin. Protein expression was induced at 37 °C with 0.1 mM isopropyl-1-thio-β-D-galactopyranoside (IPTG). Bacteria were lysed by sonication in the presence of 50 mM Tris-HCl at pH 7.6, 150 mM NaCl, 1 mM phenylmethylsulfonyl fluoride (PMSF), 5 mM ethylenediaminetetraacetic acid (EDTA), 1 mM dithiothreitol (DTT), and 1% Triton X-100. GST fusion proteins were purified over glutathione-Sepharose 4B resin (Amersham Biosciences) and were digested in column with 25 units of thrombin (Amersham Pharmacia) during 3 h at room temperature in 4 mL of Tris-NaCl buffer (TBS) and with mild shaking. Samples were then eluted, and thrombin was removed by absorption with *p*-amino-benzamidine-agarose beads (Sigma). A Centricon spin dialysis tube (5-kDa cutoff; Amicon, Inc) was used to concentrate until a 200 μL final volume was reached. Final protein concentration was determined by UV absorbance at 278 nm. The final buffer used for all NMR experiments was 50 mM Tris-HCl, 50 mM NaCl, 1 mM DTT, and 1 mM NaN_3 at pH 7.2.

NMR Spectroscopy. Protein samples were prepared at a concentration of ~1.5 mM in either 99.96% ^2H_2O or 90% H_2O and 10% ^2H_2O. NMR experiments were performed at 303 K on a Bruker DRX500 and a Bruker 600 MHz AVANCE spectrometer equipped with a triple-resonance inverse cryo-probe head. ^1H-^{15}N and ^1H-^{13}C nuclear Overhauser effect spectroscopy (NOESY)−heteronuclear multiple-quantum correlation (HMQC) spectra were collected on a Varian INOVA-800 spectrometer. NMR spectra were processed using XWINNMR (Bruker Biospin) and GIFA (*23*) software and analyzed with XEASY (*24*).

Sequential backbone assignments of TcUBP1 (ΔGQ) were obtained on scalar couplings through the backbone (*25*, *26*) using the following heteronuclear 3D spectra: HNCACB (*27*), CBCA(CO)NH (*28*), HNCA (*29*), and CA(CO)NH (*30*). This assignment was further confirmed by searching for characteristic sequential cross-peaks from the backbone amide proton to the preceding amide or a proton in an ^1H-^{15}N NOESY−HMQC experiment (*31*). Carbon and proton assignments were obtained from ^1H-^{15}N total correlation spectroscopy (TOCSY)−HMQC, HNHA (*32*), C(CO)NH, H(CCO)NH (*33*), and HNCO experiments (*34*). ^1H, ^{13}C, and ^{15}N chemical-shift assignments have been deposited in the BioMagResBank with accession number 6315. Backbone assignment of the Gly-rich region was done with the TcUBP1 (ΔNQ) recombinant protein using the HNCA experiment. Additionally, analysis of the Chemical Shift Index (CSI) in this region was complemented with the assignments of the Hα and C′ resonances from the HNHA (*32*) and HNCO experiments, respectively. As for the assignment, the two constructs TcUBP1 (ΔGQ) and TcUBP1 (ΔNQ) were used to study the backbone mobility of the different regions of the protein to minimize the cross-peak overlap of residues because of the lack of structure of the N- and C-terminal regions. Amide heteronuclear $^1H[^{15}N]$-NOEs were therefore measured at 14.1 T (600 MHz for ^1H) and 298 K (*35*).

Structure Calculations. On the basis of the almost complete assignment of ^1H, ^{13}C, and ^{15}N resonances of TcUBP1, a total of 1369 NOE distance constraints (including 376 long-range NOEs) was obtained from a 2D homonuclear NOESY recorded in D_2O and the two ^{15}N- and ^{13}C,^{15}N-edited NOESY−HMQC spectra ($\tau_m = 100$ ms). NOE analysis and assignment were performed using XEASY and ARIA (*36*). These NOE cross-peaks were unambiguously assigned after 3 rounds in ARIA of which about 150 were manually assigned. Distances involving ambiguous constraints, methyl groups, aromatic ring protons, and the non-stereospecifically assigned methylene protons were treated as the sum of separate contributions to the target function. Regions of regular α-helical and β-strand secondary structures were determined based on Cα, Hα, and CO chemical shifts (*37*), sequential and medium-range NOE patterns, and values of $^3J_{HNH\alpha}$ coupling constants derived from an HNHA experiment (*32*). From this latter experiment, 47 ϕ dihedral angles were obtained and used in the ARIA protocol.

A lyophilized sample of ^{15}N-labeled TcUBP1 (ΔGQ) was dissolved in D_2O, and ^1H-^{15}N heteronuclear single-quantum correlation (HSQC) experiments were recorded at 10 min intervals at 303 K to identify hydrogen-bond donors. The best 20 structures having the lowest energy and least violations were then used to identify the best candidate for the acceptor. For each hydrogen bond, two distance restraints were applied, 1.5−2.3 Å for NH(*i*)−O(*j*) and 2.5−3.3 Å for N(*i*)−O(*j*). A total of 27 hydrogen bonds were consistently observed giving rise to 54 distance restraints. Also, structures were used as input for the TALOS program (*38*), and 55 ϕ- and ψ-dihedral angles were unambiguously validated. A total of 20 additional ϕ-dihedral and 55 new ψ-dihedral angle constraints were consequently used in the structure calculation because 35 of the 55 validated ϕ-dihedral angles were already validated by the HNHA experiment.

This ensemble of 1423 distances and 122 dihedral restraints (Table 1) was finally used in a CNS structural calculation protocol (*39*) using standard parameters and starting with an extended molecule to generate a total of 100 final conformers of TcUBP1 (ΔQ). The 20 structures that show the lowest energy and did not show any distance constraint violation of more than 0.2 Å were used for further analysis. Geometry of the structures, structural parameters, and secondary-structure elements were analyzed and visualized using MOLMOL (*40*) and PROCHECK (*41*). The N- and C-terminus-unstructured regions 1−39 and 120−139 were not included in the analysis. The coordinates of these 20 structures have been deposited in the Protein Data Bank with accession code 1U6F.

NMR Titration with U-Rich RNA. The RNA sequence 5′-GUUUUUGUUUUUG-3′ ($\epsilon_{260} = 128\,700$ M^{-1} cm^{-1}) was titrated by NMR with the TcUBP1 (ΔNQ) protein. This RNA was synthesized and purified by the University of Calgary Regional DNA Synthesis laboratory. The oligoribonucleotide was then resuspended in buffer containing 50 mM Tris-HCl

Table 1: Experimental Restraints and Structural Statistics

number of experimental restraints	
distance restraints from NOEs	1423
intra ($i = j$)	409
sequential ($\|i - j\| = 1$)	379
medium range ($2 \leq \|i - j\| \leq 5$)	217
long range ($\|i - j\| \geq 6$)	418
hydrogen-bond restraints	54
dihedral angle restraints	122
ϕ	67
ψ	55
total experimental restraints	1599
statistics for structure calculations ($\langle SA \rangle$)	
rmsd from idealized covalent geometry	
bonds (Å)	0.0019 ± 0.0011
angles (deg)	0.3555 ± 0.0098
improper (deg)	0.2563 ± 0.0146
rmsd from experimental data	
NOEs (Å)	0.0142 ± 0.0012
dihedrals (deg)	0.5023 ± 0.0427
Ramachandran analysis (%)[a]	
residues in favored regions	82.8 ± 2.0
residues in additional allowed regions	16.1 ± 2.7
residues in generously allowed regions	1.1 ± 1.0
residues in disallowed regions	0.0 ± 0.0

[a] Generated using PROCHECK on the ensemble of the 20 lowest-energy structures, residues 40−119.

at pH 7.2 and 50 mM NaCl. The RNase inhibitors, Rnasin (Promega) (2%, v/v) and Heparin (Sigma) (500 μg/mL), were added to prevent RNA degradation. The pH of the RNA solution was adjusted to 7.2 by addition of NaOH. HSQC titration experiments were carried out by adding increasing concentrations of the RNA oligonucleotide to a 0.4 mM [U-^{15}N]-labeled protein solution to reach the final 1:2 ratio of protein/RNA.

ITC. Experiments were carried out on a MicroCal VP-ITC titration calorimeter (MicroCal Inc., Northampton, MA) using the VPViewer software for instrument control and data acquisition. The buffer used for ITC experiments was the same as for NMR. The experiments were performed at a constant temperature (15 °C) by titrating TcUBP1 (ΔNQ) or TcUBP1 (ΔNGQ) in a stirred reaction cell of 1.4 mL. A total of 38 injections each of 8 μL volume and 16 s duration, with a 5 min interval between each injections, were carried out using a 300 μL syringe filled with the RNA. Titration experiments were performed with ∼0.11 mM TcUBP1 solutions in the cell and 1.0 mM RNA solution in the syringe to ensure a final RNA/TcUBP1 ratio of 2.25:1 in the reaction cell. The different solutions and buffer solutions were thoroughly degassed by stirring under vacuum before ITC measurements. The calorimetric data were processed using the software package ORIGIN (version 7.0) provided by the manufacturer. The binding isotherm was fit by an iterative nonlinear least-squares algorithm (Marquadt method) to a binding model employing a single set of independent sites. The binding constant (K_d), molar binding stoichiometry (N), molar binding entropy (ΔS_o), and molar binding enthalpy (ΔH_o) were determined directly from the fitted curve.

RESULTS

Structure Determination. Different two- and three-dimensional NMR spectra were recorded on TcUBP1 (ΔGQ) and TcUBP1 (ΔNQ) (residues 1−139 and 35−156, respectively) to assign their ^{1}H, ^{15}N, and ^{13}C resonances. All of the peaks corresponding to residues 38−137 were perfectly superimposable in the ^{1}H-^{15}N HSQC of both protein fragments. Around 50% of the backbone and side-chain resonances were assigned in the auxiliary regions (N-terminal, variable, and Gly-rich regions), while almost all of the ^{1}H, ^{15}N, and ^{13}C signal assignments were obtained for the structured region of the protein from residue Val^{41} to Ala^{120}. This was straightforward because of the good dispersion of the cross-peaks in the ^{15}N and ^{13}C HSQC and the excellent magnetization transfer observed in the ^{1}H-^{15}N TOCSY−HMQC, C(CO)NH, and H(CCO)NH experiments. Assignment of certain aliphatic protons was achieved using the strong intra- and sequential NOEs in the ^{1}H-^{13}C-NOESY−HMQC, and aromatic side-chain protons assignments were confirmed from a 2D homonuclear NOESY in D_2O. Four amides corresponding to residues Thr^{52}, Gln^{58}, Leu^{59}, and Ser^{95} were not detected in the ^{15}N-HSQC most likely because of exchange broadening, but their side chains were partially assigned using NOEs from the neighboring residues. As a consequence, a high number of distance restraints were

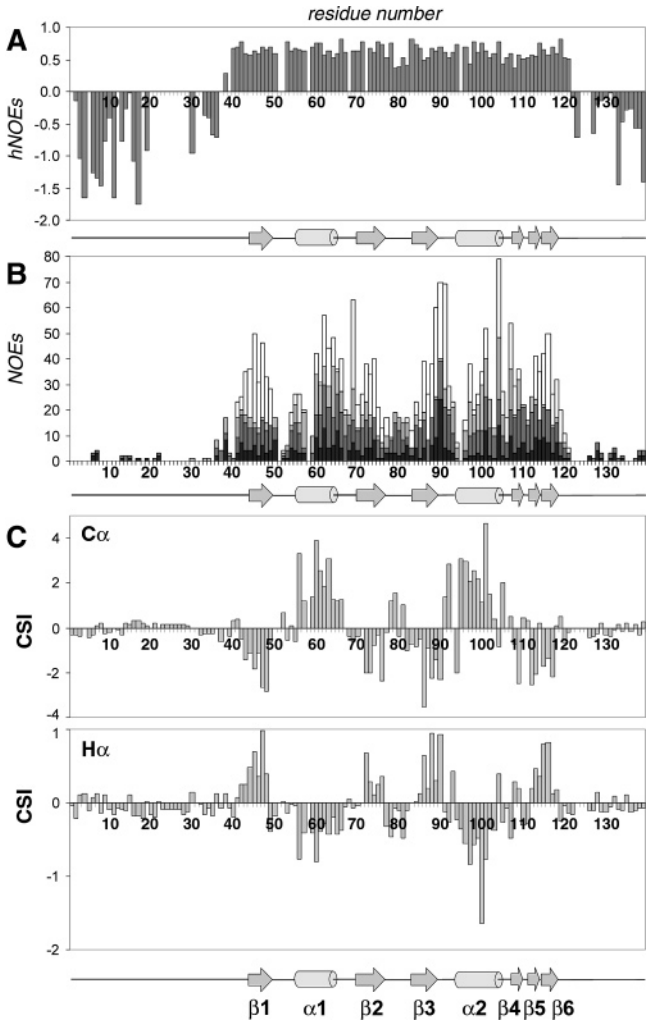

FIGURE 2: (A) Measured heteronuclear ^{15}N[^{1}H]-NOE (hNOEs) values obtained for the amide backbone groups of TcUBP1 (ΔGQ). No values are shown for prolines and residues with peaks that cannot be accurately quantitated because of spectral overlap. (B) Number of NOE restraints per residue for the NMR structure of TcUBP1 (ΔGQ) (intraresidual, sequential, and medium- and long-range for dark- to light-colored bars). (C) CSI analysis for the Cα and Hα resonances. The α and β secondary-structure elements are indicated.

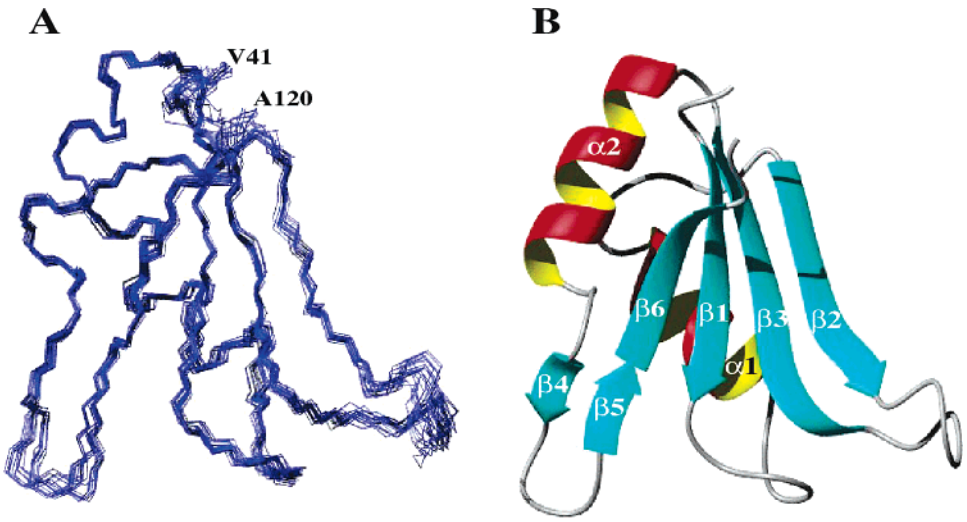

FIGURE 3: Structure of the RRM domain of TcUBP1. (A) Backbone traces of the 20 lowest energy structures of TcUBP1 (ΔGQ) superimposed using backbone atoms from Val[41] to Ala[120]. (B) Ribbon diagram of the minimized mean structure. Secondary-structure elements are labeled as described in the text.

obtained (18.9 restraints per residue including dihedral restraints) and used in the structure calculation of TcUBP1 (ΔGQ). Structural statistics for the best 20 structures are given in Table 1.

Solution Structure of TcUBP1 (ΔGQ). As expected, the N- and the C-terminal regions of TcUBP1 (ΔGQ) were unfolded in solution as shown by the negative values of the heteronuclear NOEs in these regions (Figure 2A), the lack of structurally relevant NOEs (Figure 2B), Cα and Hα secondary chemical shifts (Figure 2C), and qualitative ^{2}H-exchange experiments. The same observation was made for the Gly-rich region in TcUBP1 (ΔNQ) (data not shown). When the folded part of the molecule is concerned, it shares the same three-dimensional structure as the other RRM-containing proteins [such as PTB, PABP1, and sex-lethal protein (Sxl), among others] with a four-stranded β sheet packed against two α helices (Figures 2C and 3) (*42*). The two α helices also have similar perpendicular orientations relative to each other. The hydrophobic core is stabilized by residues Leu[45], Val[47], Ile[50], Leu[59], Leu[62], Phe[63], Tyr[66], Val[72], Ile[74], Val[89], Phe[91], Ala[100], Leu[104], Phe[107], Ile[109], Leu[114], Val[116], and Leu[118], while positive and negative charges are spread out around the molecule. One can notice the presence of a β-hairpin motif between α2 and β6 that is observed in some other RRMs of hnRNP A1 (*43*), Hu protein (HuD) (*10*), and U2AF proteins (*44*). This β hairpin is stabilized by two backbone hydrogen bonds between residues Phe[107] and Leu[114]. The global structure of this part of TcUBP1 appears quite rigid and exhibits an root-mean-square deviation (rmsd) of only 0.46 ± 0.15 Å for backbone heavy atoms and 0.96 ± 0.18 Å for all heavy atoms. The regions that are less rigid are the loops between β2 and β3 and the β hairpin between α2 and β6 (Figures 2A and 3A).

NMR Mapping of the RNA-Binding Surface. Amide chemical-shift perturbations were used to identify residues that interact with RNA. This sensitive method gives qualitative information about the site of binding and affinity. During titration of TcUBP1 (ΔNQ) with RNA, we observed that most of the backbone ^{1}H-^{15}N resonances shifted in a continuous manner with no obvious exchange broadening, indicative of fast exchange on the NMR time scale between the bound and free states of the protein (Figure 4B). This is consistent with a micromolar dissociation constant (K_d). Several residues, Leu[45], Asn[48], and Tyr[49] (β-strand 1) and Gly[106], Ile[109], Asn[111], Arg[113], Leu[114], and Lys[115] (β-hairpin β4−β5), displayed exchange broadening in the NMR spectra (Figure 4C), indicative of solvent exchange or more complicated exchange behavior in the bound state. These results are consistent with an ITC experiment that measured a K_d of 16.6 ± 0.1 μM between TcUBP1 (ΔNQ) and the same GU-rich RNA (Figure 5).

The RNA sequence that we used in our NMR titration (5′-GUUUUUGUUUUUG-3′) was chosen because it was found to be the minimal sequence capable to bind specifically TcUBP1 (*20*, *22*). This single-stranded 13-mer is derived from the mucin *TcSMUG* 3′ UTR, with adenosines replaced by guanosines. Previous results had shown that GU-rich sequences are better substrates for TcUBP1 binding than AU sequences (*20*). The chemical-shift differences between free and RNA-bound TcUBP1 (ΔNQ) show that the RRM β-sheet surface is mainly involved in this interaction (Figure 6A). The distribution of these perturbations is shown on the three-dimensional solution structure of the free form of TcUBP1 in Figure 6B. The C-terminal extension comprising the variable and the Gly-rich regions also shows some chemical-shift differences but to a lesser extent. We also remarked significant chemical-shift perturbations for the two Asn[44] and Asn[48] side-chain amide groups that are both located on the β1 strand (in the RNP2 motif). Finally, the β hairpin that protrudes between α2 and β6 appears to play a significant role in RNA recognition because a large number of residues from Gly[106] to Gly[122] were more or less affected by this binding. Several of these resonances were severely broadened. Small chemical-shift changes were also observed for the side-chain amide groups of Asn[108] and Asn[111].

The ITC experiment showed that RNA binding is driven by a large negative enthalpy change (−38.1 ± 1.5 kcal mol^{-1}), suggesting the formation of hydrogen bonds, van der Waals contacts, and/or electrostatic interactions. Given the polar and charged nature of RNA, it is likely that hydrogen-bond/electrostatic interactions contribute significantly to the binding reaction. Binding was accompanied by

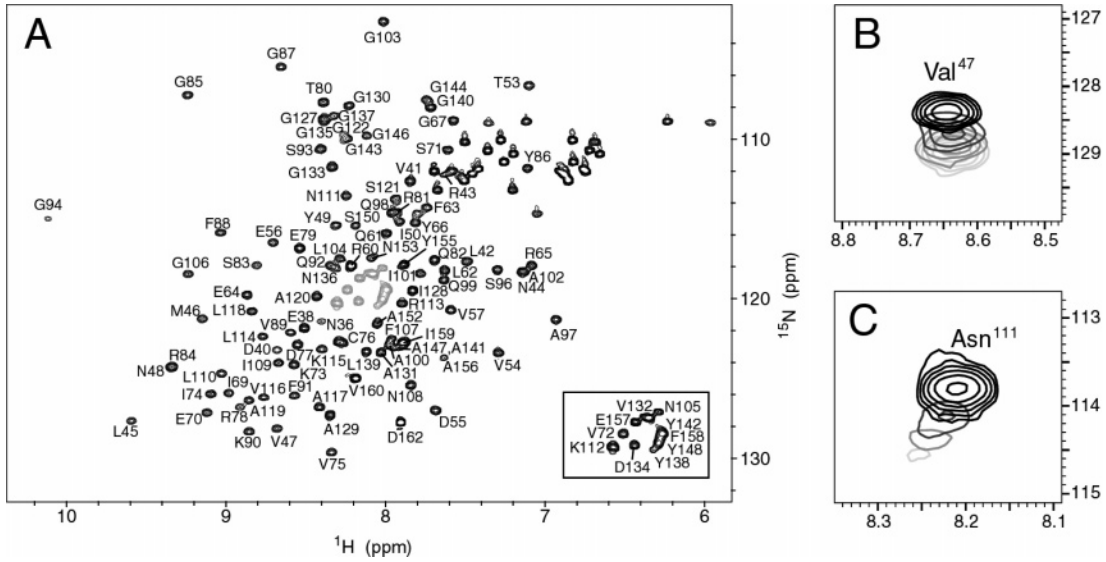

FIGURE 4: (A) Two-dimensional ^{1}H-^{15}N-HSQC spectrum of the uniformly ^{15}N-labeled TcUBP1 (ΔNQ). Unlabeled cross-peaks are the NH_2 groups of the Asn and Gln side chains. For clarity, cross-peak assignments in the central region of the spectrum (shown in gray) are shown in the box at the bottom right. Changes in the ^{1}H-^{15}N-HSQC cross-peaks upon addition of the RNA 13-mer 5′-GUUUUUGUUUUUG-3′ showing residues in fast exchange (B) and exchange broadened (C) at [protein]/[RNA] ratios of 1:0, 1:0.3, 1:0.7, and 1:1, color coded from black (1:0) to light gray (1:1).

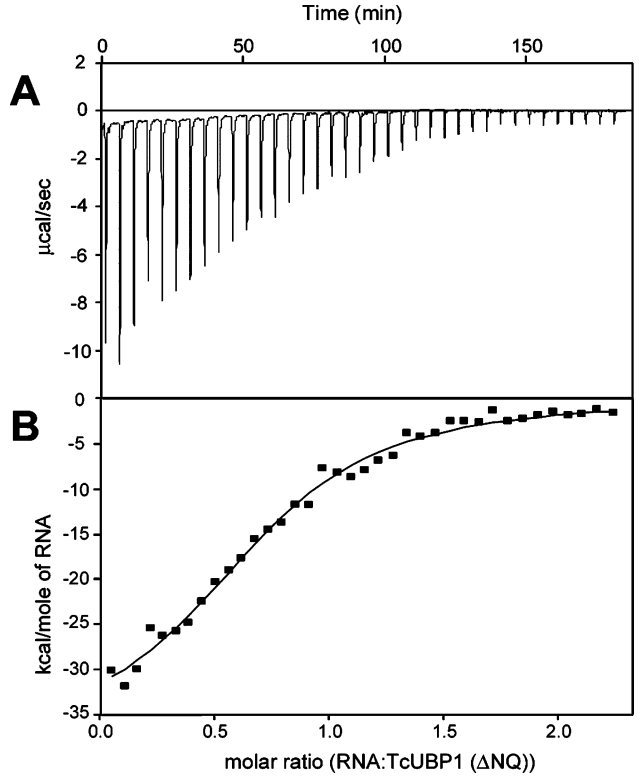

FIGURE 5: ITC data of RNA binding to TcUBP1 (ΔNQ). (A) Calorimetric titration profile of aliquots of the 13-mer GU-rich RNA (1.0 mM) injected into 0.12 mM TcUBP1 (ΔNQ) at 15 °C. (B) Continuous line represents the least-squares fit of the data of the heat absorbed per mole of titrant as a function of the molar ratio using a one-site model.

a large negative entropy change (−119 cal mol^{-1} K^{-1}), indicating an increase in order during the RNA binding. The larger negative enthalpy term (Δ*H*), relative to the entropic contribution (Δ*S*), leads to a favorable free energy (Δ*G*) of binding of −6.4 ± 0.9 kcal mol^{-1} (Figure 5).

A second ITC experiment was carried out with TcUBP1 (ΔNGQ), residues 35−139. Very similar thermodynamic parameters were found for the protein lacking the Gly-rich region: the K_d was 14.3 ± 0.1 μM, and the other parameters were an enthalpy (Δ*H*) of −40.8 ± 1.5 kcal mol^{-1} and entropy (Δ*S*) of −110 cal mol^{-1} K^{-1}. This supports the previous finding that the ∼92 amino acid RRM domain is sufficient for RNA binding (*22*).

A Model for the RRM Interaction with RNA. Although we did not determine the structure of the TcUBP1/RNA complex, we modeled the TcUBP1/RNA complex using the HADDOCK software (*45*) and the HuD (RRM1)/RNA (5′-UUUUAUUU-3′) complex (*10*) (Figure 7). On the basis of the NMR studies in this work, we can assume the participation of the side chain of Lys^{115} (β5) but also of the main-chain atoms of Arg^{113} (β5) and Ala^{120} (β6), which show large chemical changes upon RNA binding (Figure 6A). Other residues in the β hairpin are also likely to be part of the RNA-binding surface, but no restraints were applied for that part of the protein. Also, we suggest that Phe^{88}, which is conserved in all RNP1 motifs (Figure 6A), makes stacking interactions with the pyrimidine base of the nucleic acid residue U10 (parts C and E of Figure 7). The side chain of Arg^{84} (equivalent to Arg^{55} in hnRNPA1) also likely interacts with RNA phosphates (Figure 6). Surprisingly, the loop connecting β2 and β3, which was shown to confer specificity for RNA binding in U1A (*42*, *46*, *47*), shows very few chemical-shift perturbations in our NMR titration experiment. In studies of Sxl-RBD1+2, the β2−β3 loop was also significantly affected by RNA binding (*48*).

For the structural modeling, we used restraints for the side chains of the following residues: Asn^{44}, Asn^{48}, Tyr^{49}, Lys^{73}, Phe^{88}, Lys^{112}, and Lys^{115} and for main-chain atoms of residues Arg^{113} and Ala^{120} (Figure 7E). The same RNA 5′−3′ orientation was chosen as in the HuD/RNA structure with the central purine base (Ade) replaced in our model by Gua^{7}. In the resulting model, all of the applied restraints were satisfied with low calculated energy. The first uracil bases were found to interact with the side-chain amide groups of Asn^{108} and Asn^{111} and also with the positively charged side

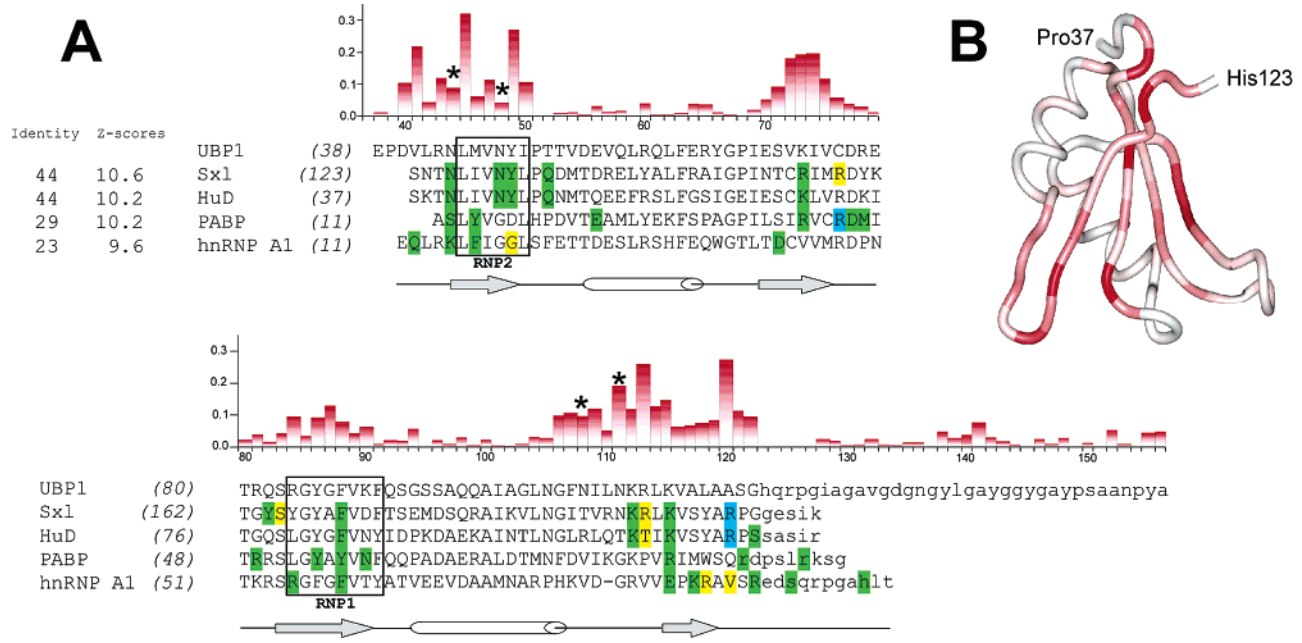

FIGURE 6: (A) Sequence alignment of TcUBP1 with the N-terminal RRM domains of the structurally related proteins Sxl, HuD, PABP1, and hnRNP A1 also called UP1 (PDB codes 1B7F, 1FXL, 1CVJ, and 2UP1, respectively). Their sequences were aligned with TcUBP1 based on primary sequences, and their identity (in percentage) and DALI *Z* score are indicated on the left. Positions that do not structurally align with TcUBP1 are indicated in lowercase letters. Residues making side-chain−RNA contacts are in green, making main-chain−RNA contacts in yellow, and making both main- and side-chain−RNA contacts in blue. The RNP1 and RNP2 motifs and the secondary structures are shown. Chemical-shift perturbations induced by the binding of RNA to TcUBP1 (ΔNQ) are shown above the sequences. The deviations (in parts per million) were quantified with the formula $\Delta = ((\delta^1\mathrm{H})^2 + (0.2\delta^{15}\mathrm{N})^2)^{1/2}$, where δ^1H and δ^{15}N are the chemical-shift differences of the amide proton and nitrogen. The side-chain amide groups perturbed during the NMR titration are identified with asterisks. (B) Amide chemical-shift perturbations mapped onto the backbone trace of the TcUBP1 RRM domain.

chain of Arg[113]. These interactions rationalize the ITC results and explain the large negative enthalpy (ΔH), which arises from the high proportion of hydrogen-bond/electrostatic interactions present in the protein−RNA complex. The negative entropy (ΔS) is due to the reduction in the translational and rotational degrees of freedom of the RNA and the protein side chains engaged in complex formation.

DISCUSSION

As expected from the sequence analysis, a DALI search (*49*) for protein structures with similar folds identified 11 RRM domains with *Z* scores above 4.0. The highest *Z* scores were from Sxl (*50*), HuD (*10*), PABP (*51*), and hnRNP A1 (*17*) (Figure 6A). The folded part of TcUBP1 exhibits the classical βαββαβ topology of the RRM family (for a review, see ref *18*), devoid of any extra N- or C-terminal secondary-structure elements as observed in some RBPs, such as the short N-terminal helix in CstF-64 (*52*) and hnRNP A1 (*43*), the C-terminal α helix in CstF-64 and U1A (*53*), the C-terminal β strand in the third RRM (RRM3) of the polypyrimidine-tract-binding protein (PTB) (*54*), or the C-terminal β strand and a long α helix in the human La protein (*55*).

TcUBP1 does contain an extra β-hairpin β4−β5, which increases the width of the β-sheet surface and appears to play a role in RNA recognition. This region is very basic and shows significant perturbations upon RNA binding. TcUBP1 is the first protein showing an enhanced contribution of this hairpin (e.g., from the β4 strand). In the crystal structures of HuD RRM1−RRM2 complexed with AUUUUUAUUUU (*10*) or Sxl RRM1−RRM2 complexed with GUUGUUUUUUUU (*50*), the RNA does not interact with this β-hairpin loop in the N-terminal RRM1 domain but rather interacts with the β sheet of RRM2 (*10*) (parts A and B of Figure 7). As a result, the β-hairpin loops are exposed to the solvent. In TcUBP1, the absence of a second RRM is likely responsible for the enhanced importance of the β hairpin in interacting with the RNA (see Figure 7E). Modeling suggests that seven nucleic acid bases are involved in TcUBP1 recognition, while eight bases are usually found to interact with proteins containing two RRMs (*10*).

A second difference observed in the TcUBP1 structure concerns the residues in the RNP1 sequence in the β3 strand, which exhibit smaller chemical-shift perturbations relative to residues in stands β1, β2, and β4. In the HuD/RNA and Sxl/RNA complexes, the bases of Ade[7] and Ura[8] respectively are both close to the β3 strand even if they make side-chain contacts with a glutamine residue (Gln[134] in Sxl and Gln[48] in HuD) located after the β1 strand (corresponding to Thr[52] in TcUBP1, Figure 6A). The absence of these glutamine-mediated interactions in TcUBP1 prevents contact with the RNA, leading to a change in the recognition in this part of the protein.

Also worth discussing are the N- and C-terminal residues within the RRM domain. As shown in Figure 6, in known structures, the residues preceding β1 and following β6 make contacts via side- and main-chain atoms with the bound RNA. A similar situation could exist in TcUBP1, but it is not clear to what extent the C-terminal residues interact with the RNA because backbone assignments were not possible for residues His[123]-Arg[125]. The large chemical-shift changes observed for the N-terminal residues Asp[40] and Val[41] suggest a direct interaction with the RNA or significant structural change in the immediate (local) environment.

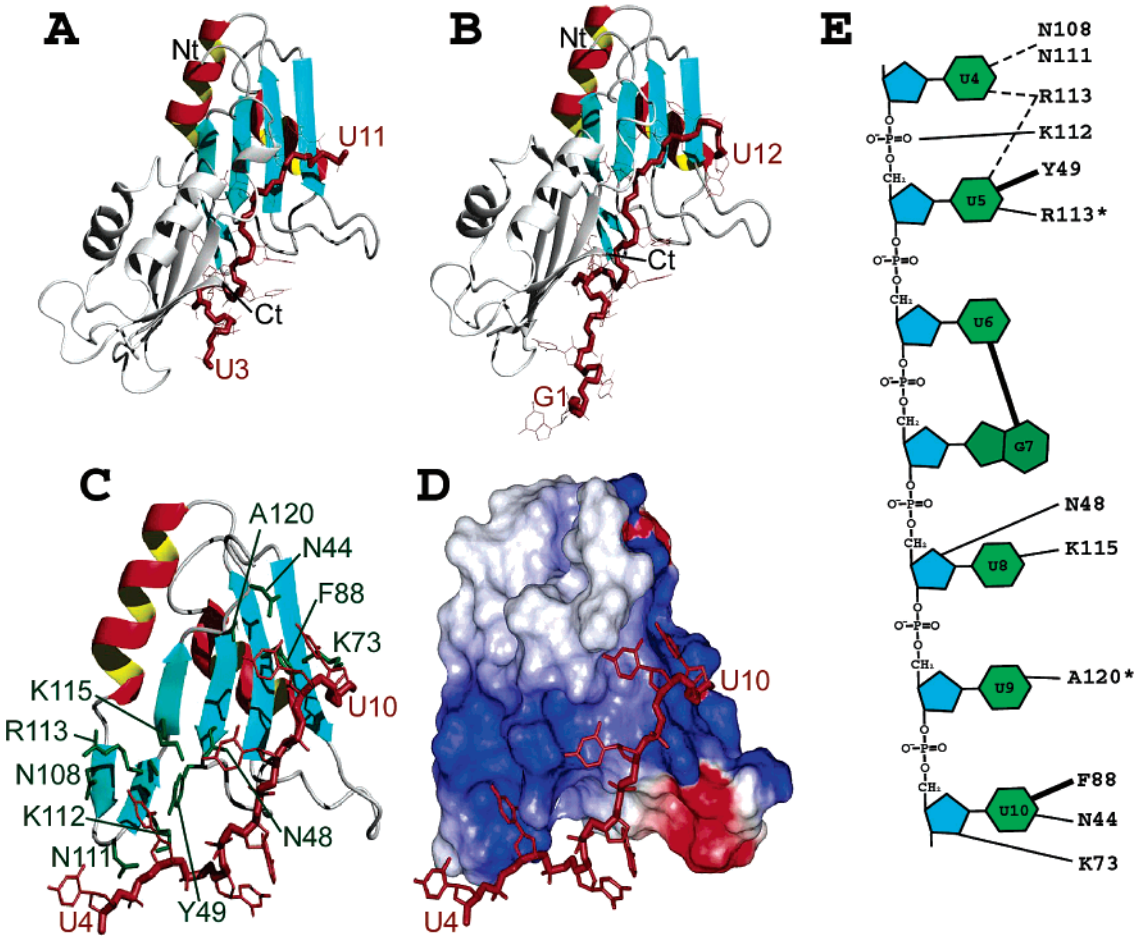

FIGURE 7: Nucleic acid recognition by RRM domains. Structures of HuD (A) and Sxl (B) in complex with U-rich RNA. The second RRM is in gray, and the RNA is in brown. (C) Model of the complex between TcUBP1 and the RNA 5′-GUUUUUGUUUUUG-3′. For greater clarity, only protein residues 40−120 and nucleic acid residues 4−10 are shown. (D) Electrostatic potential of the TcUBP1 RRM surface. The surface is color-coded with red indicating negative potential and blue indicating positive potential. (E) Summary of expected contacts between TcUBP1 and the RNA fragment. Thick lines indicate stacking interactions, and dashed lines indicate interactions observed in certain parts of the calculated models. An asterisk is shown for residues making main-chain contacts with the RNA.

In higher eukaryotic RBPs that contain multiple RRM domains, the first and second RRMs are often the most important in term of RNA binding (*10*, *56*). Accessory functions, such as localization, oligomerization, and protein−protein interaction (*57*−*59*), and structural stability (*53*) have been attributed to the following RRMs. Here, we show that the RNA-binding affinity of TcUBP1 (ΔNQ) is in the micromolar range, which is in agreement with the previous studies of other individual RRMs. The presence of two or more domains is required for higher affinity (*48*, *60*). At present, all of the known RRM/RNA complex structures are from proteins containing at least two RRMs. Relevant previous structural studies of complexes involving U-rich RNA fragments are NMR titration experiments with (i) RRM1 of hnRNP C and a U_8 RNA (*61*), (ii) RRM2 of Sxl and GU_8 (*62*), and (iii) RRM1 and RRM2 of HuC and a AUUUA RNA (*60*). To our knowledge, TcUBP1 is the first NMR structure of an RRM domain from a lower eukaryotic protein that contains a single RRM domain.

Single RRM proteins often contain auxiliary domains that are involved in protein−protein associations. In the case of TcUBP1/2, the Gly-rich auxiliary region was found to be crucial for the dimerization and the variable region was shown to be related to the RNA-binding mode (*22*). This previous study showed that TcUBP1 can interact *in vivo* with TcUBP2 and that this heterodimer is detected in the cell as a preformed heterodimer that does not bind RNA. The RRM domain of TcUBP2 differs from TcUBP1 only in two residues (Val^{41} and Cys^{76} instead of Leu^{27} and Ala^{62}) and binds RNA with comparable affinity (*22*). Our structure of TcUBP1 provides a starting point for understanding the precise role of the heterodimerization that occurs between TcUBP1 and TcUBP2 in the destabilization process of *TcSMUG* RNA.

ACKNOWLEDGMENT

We thank the Canadian National High Field NMR Center (NANUC) for their assistance and use of the facilities.

REFERENCES

1. de Souza, W. (1999) A short review on the morphology of *Trypanosoma cruzi*: From 1909 to 1999, *Mem. Inst. Oswaldo Cruz 94*, Suppl. 1, 17−36.
2. Matthews, K. R., Tschudi, C., and Ullu, E. (1994) A common pyrimidine-rich motif governs trans-splicing and polyadenylation of tubulin polycistronic pre-mRNA in trypanosomes, *Genes Dev. 8*, 491−501.
3. Clayton, C. E. (2002) Life without transcriptional control? From fly to man and back again, *EMBO J. 21*, 1881−1888.
4. Wickens, M., Anderson, P., and Jackson, R. J. (1997) Life and death in the cytoplasm: Messages from the 3′ end, *Curr. Opin. Genet. Dev. 7*, 220−232.

5. D'Orso, I., De Gaudenzi, J. G., and Frasch, A. C. (2003) RNA-binding proteins and mRNA turnover in trypanosomes, *Trends Parasitol. 19*, 151−155.
6. Caput, D., Beutler, B., Hartog, K., Thayer, R., Brown-Shimer, S., and Cerami, A. (1986) Identification of a common nucleotide sequence in the 3′-untranslated region of mRNA molecules specifying inflammatory mediators, *Proc. Natl. Acad. Sci. U.S.A. 83*, 1670−1674.
7. Shaw, G., and Kamen, R. (1986) A conserved AU sequence from the 3′ untranslated region of GM-CSF mRNA mediates selective mRNA degradation, *Cell 46*, 659−667.
8. Antic, D., and Keene, J. D. (1997) Embryonic lethal abnormal visual RNA-binding proteins involved in growth, differentiation, and posttranscriptional gene expression, *Am. J. Hum. Genet. 61*, 273−278.
9. Wakamatsu, Y., and Weston, J. A. (1997) Sequential expression and role of Hu RNA-binding proteins during neurogenesis, *Development 124*, 3449−3460.
10. Wang, X., and Hall, T. M. (2001) Structural basis for recognition of AU-rich element RNA by the HuD protein, *Nat. Struct. Biol. 8*, 141−145.
11. Perrone-Bizzozero, N., and Bolognani, F. (2002) Role of HuD and other RNA-binding proteins in neural development and plasticity, *J. Neurosci. Res. 68*, 121−126.
12. Gunderson, S. I., Vagner, S., Polycarpou-Schwarz, M., and Mattaj, I. W. (1997) Involvement of the carboxyl terminus of vertebrate poly(A) polymerase in U1A autoregulation and in the coupling of splicing and polyadenylation, *Genes Dev. 11*, 761−773.
13. Boelens, W. C., Jansen, E. J., van Venrooij, W. J., Stripecke, R., Mattaj, I. W., and Gunderson, S. I. (1993) The human U1 snRNP-specific U1A protein inhibits polyadenylation of its own pre-mRNA, *Cell 72*, 881−892.
14. van Gelder, C. W., Gunderson, S. I., Jansen, E. J., Boelens, W. C., Polycarpou-Schwarz, M., Mattaj, I. W., and van Venrooij, W. J. (1993) A complex secondary structure in U1A pre-mRNA that binds two molecules of U1A protein is required for regulation of polyadenylation, *EMBO J. 12*, 5191−5200.
15. Varani, L., Gunderson, S. I., Mattaj, I. W., Kay, L. E., Neuhaus, D., and Varani, G. (2000) The NMR structure of the 38 kDa U1A protein−PIE RNA complex reveals the basis of cooperativity in regulation of polyadenylation by human U1A protein, *Nat. Struct. Biol. 7*, 329−335.
16. Hamilton, B. J., Nagy, E., Malter, J. S., Arrick, B. A., and Rigby, W. F. (1993) Association of heterogeneous nuclear ribonucleoprotein A1 and C proteins with reiterated AUUUA sequences, *J. Biol. Chem. 268*, 8881−8887.
17. Ding, J., Hayashi, M. K., Zhang, Y., Manche, L., Krainer, A. R., and Xu, R. M. (1999) Crystal structure of the two-RRM domain of hnRNP A1 (UP1) complexed with single-stranded telomeric DNA, *Genes Dev. 13*, 1102−1115.
18. Antson, A. A. (2000) Single-stranded-RNA binding proteins, *Curr. Opin. Struct. Biol. 10*, 87−94.
19. Burd, C. G., and Dreyfuss, G. (1994) Conserved structures and diversity of functions of RNA-binding proteins, *Science 265*, 615−621.
20. D'Orso, I., and Frasch, A. C. (2001) TcUBP-1, a developmentally regulated U-rich RNA-binding protein involved in selective mRNA destabilization in trypanosomes, *J. Biol. Chem. 276*, 34801−34809.
21. De Gaudenzi, J. G., D'Orso, I., and Frasch, A. C. (2003) RNA recognition motif-type RNA-binding proteins in *Trypanosoma cruzi* form a family involved in the interaction with specific transcripts *in vivo*, *J. Biol. Chem. 278*, 18884−18894.
22. D'Orso, I., and Frasch, A. C. (2002) TcUBP-1, an mRNA destabilizing factor from trypanosomes, homodimerizes and interacts with novel AU-rich element- and Poly(A)-binding proteins forming a ribonucleoprotein complex, *J. Biol. Chem. 277*, 50520−50528.
23. Pons, J. L., Malliavin, T. E., and Delsuc, M. A. (1996) Gifa V.4: A complete package for NMR dataset processing, *J. Biomol. NMR 8*, 445−452.
24. Bartels, C., Xia, T.-H., Billeter, M., Güntert, P., and Wüthrich, K. (1995) The program XEASY for computer-supported NMR spectral analysis of biological macromolecules, *J. Biomol. NMR 5*, 1−10.
25. Kay, L. E., Ikura, M., Tschudin, R., and Bax, A. (1990) Three-dimensional triple resonance NMR-spectroscopy of isotopically enriched proteins, *J. Magn. Reson. 89*, 496−514.
26. Kay, L. E. (1997) NMR methods for the study of protein structure and dynamics, *Biochem. Cell Biol. 75*, 1−15.
27. Wittekind, M., and Mueller, L. (1993) HNCACB, a high sensitivity 3D NMR experiment to correlate amide-proton and nitrogen resonances with the α and β carbon resonances in proteins, *J. Magn. Reson. B 101*, 201−205.
28. Grzesiek, S., and Bax, A. (1992) Correlating backbone amide and side chain resonances in larger proteins by multiple relayed triple resonance NMR, *J. Am. Chem. Soc. 114*, 6291−6293.
29. Farmer, B. T., II, Venters, R. A., Spicer, L. D., Wittekind, M. G., and Mueller, L. (1992) A refocused and optimized HNCA: Increased sensitivity and resolution in large macromolecules, *J. Biomol. NMR 2*, 195−202.
30. Bax, A., and Ikura, M. (1991) An efficient 3D NMR technique for correlating the proton and ^{15}N backbone amide resonances with the α-carbon of the preceding residue in uniformly ^{15}N/^{13}C-enriched proteins, *J. Biomol. NMR 1*, 99−104.
31. Wüthrich, K. (1986) *NMR of Proteins and Nucleic Acids*, Wiley-Interscience, New York.
32. Kuboniwa, H., Grzesiek, S., Delaglio, F., and Bax, A. (1994) Measurement of HN−H α J couplings in calcium-free calmodulin using new 2D and 3D water-flip-back methods, *J. Biomol. NMR 4*, 871−878.
33. Grzesiek, S., Anglister, J., and Bax, A. (1993) Correlation of backbone amide and aliphatic side-chain resonances in ^{13}C/^{15}N-enriched proteins by isotropic mixing of ^{13}C magnetization, *J. Magn. Reson. 101*, 114−119.
34. Grzesiek, S., and Bax, A. (1992) Improved 3D triple-resonance NMR techniques applied to a 31 kDa protein, *J. Magn. Reson. 96*, 432−440.
35. Peng, J. W., and Wagner, G. (1994) Investigation of protein motions via relaxation measurements, *Methods Enzymol. 239*, 563−596.
36. Nilges, M., Macias, M. J., O'Donoghue, S. I., and Oschkinat, H. (1997) Automated NOESY interpretation with ambiguous distance restraints: The refined NMR solution structure of the pleckstrin homology domain from β-spectrin, *J. Mol. Biol. 269*, 408−422.
37. Wishart, D. S., and Sykes, B. D. (1994) The ^{13}C chemical-shift index: A simple method for the identification of protein secondary structure using ^{13}C chemical-shift data, *J. Biomol. NMR 4*, 171−180.
38. Cornilescu, G., Delaglio, F., and Bax, A. (1999) Protein backbone angle restraints from searching a database for chemical shift and sequence homology, *J. Biomol. NMR 13*, 289−302.
39. Brunger, A. T., Adams, P. D., Clore, G. M., DeLano, W. L., Gros, P., Grosse-Kunstleve, R. W., Jiang, J. S., Kuszewski, J., Nilges, M., Pannu, N. S., Read, R. J., Rice, L. M., Simonson, T., and Warren, G. L. (1998) Crystallography and NMR system: A new software suite for macromolecular structure determination, *Acta Crystallogr., Sect. D 54* (Part 5), 905−921.
40. Koradi, R., Billeter, M., and Wüthrich, K. (1996) MOLMOL: A program for display and analysis of macromolecular structures, *J. Mol. Graphics 14*, 51−55, 29−32.
41. Laskowski, R. A., MacArthur, M. W., Moss, D. S., and Thornton, J. M. (1993) PROCHECK: A program to check the stereochemical quality of protein structures, *J. Appl. Crystallogr. 26*, 283−291.
42. Nagai, K., Oubridge, C., Jessen, T. H., Li, J., and Evans, P. R. (1990) Crystal structure of the RNA-binding domain of the U1 small nuclear ribonucleoprotein A, *Nature 348*, 515−520.
43. Shamoo, Y., Krueger, U., Rice, L. M., Williams, K. R., and Steitz, T. A. (1997) Crystal structure of the two RNA binding domains of human hnRNP A1 at 1.75 Å resolution, *Nat. Struct. Biol. 4*, 215−222.
44. Kielkopf, C. L., Rodionova, N. A., Green, M. R., and Burley, S. K. (2001) A novel peptide recognition mode revealed by the X-ray structure of a core U2AF35/U2AF65 heterodimer, *Cell 106*, 595−605.
45. Dominguez, C., Boelens, R., and Bonvin, A. M. (2003) HADDOCK: A protein−protein docking approach based on biochemical or biophysical information, *J. Am. Chem. Soc. 125*, 1731−1737.
46. Jessen, T. H., Oubridge, C., Teo, C. H., Pritchard, C., and Nagai, K. (1991) Identification of molecular contacts between the U1 A small nuclear ribonucleoprotein and U1 RNA, *EMBO J. 10*, 3447−3456.
47. Scherly, D., Boelens, W., Dathan, N. A., van Venrooij, W. J., and Mattaj, I. W. (1990) Major determinants of the specificity of

interaction between small nuclear ribonucleoproteins U1A and U2B″ and their cognate RNAs, *Nature 345*, 502−506.
48. Lee, A. L., Volkman, B. F., Robertson, S. A., Rudner, D. Z., Barbash, D. A., Cline, T. W., Kanaar, R., Rio, D. C., and Wemmer, D. E. (1997) Chemical shift mapping of the RNA-binding interface of the multiple-RBD protein sex-lethal, *Biochemistry 36*, 14306−14317.
49. Holm, L., and Sander, C. (1994) The FSSP database of structurally aligned protein fold families, *Nucleic Acids Res. 22*, 3600−3609.
50. Handa, N., Nureki, O., Kurimoto, K., Kim, I., Sakamoto, H., Shimura, Y., Muto, Y., and Yokoyama, S. (1999) Structural basis for recognition of the *tra* mRNA precursor by the sex-lethal protein, *Nature 398*, 579−585.
51. Deo, R. C., Bonanno, J. B., Sonenberg, N., and Burley, S. K. (1999) Recognition of polyadenylate RNA by the poly(A)-binding protein, *Cell 98*, 835−845.
52. Perez Canadillas, J. M., and Varani, G. (2003) Recognition of GU-rich polyadenylation regulatory elements by human CstF-64 protein, *EMBO J. 22*, 2821−2830.
53. Avis, J. M., Allain, F. H., Howe, P. W., Varani, G., Nagai, K., and Neuhaus, D. (1996) Solution structure of the N-terminal RNP domain of U1A protein: The role of C-terminal residues in structure stability and RNA binding, *J. Mol. Biol. 257*, 398−411.
54. Conte, M. R., Grune, T., Ghuman, J., Kelly, G., Ladas, A., Matthews, S., and Curry, S. (2000) Structure of tandem RNA recognition motifs from polypyrimidine tract binding protein reveals novel features of the RRM fold, *EMBO J. 19*, 3132−3141.
55. Jacks, A., Babon, J., Kelly, G., Manolaridis, I., Cary, P. D., Curry, S., and Conte, M. R. (2003) Structure of the C-terminal domain of human La protein reveals a novel RNA recognition motif coupled to a helical nuclear retention element, *Structure 11*, 833−843.
56. Varani, G. (2001) Delivering messages from the 3′ end, *Proc. Natl. Acad. Sci. U.S.A. 98*, 4288−4289.
57. Perez, I., McAfee, J. G., and Patton, J. G. (1997) Multiple RRMs contribute to RNA binding specificity and affinity for polypyrimidine tract binding protein, *Biochemistry 36*, 11881−11890.
58. Khaleghpour, K., Kahvejian, A., De Crescenzo, G., Roy, G., Svitkin, Y. V., Imataka, H., O'Connor-McCourt, M., and Sonenberg, N. (2001) Dual interactions of the translational repressor Paip2 with poly(A) binding protein, *Mol. Cell. Biol. 21*, 5200−5213.
59. Kielkopf, C. L., Lucke, S., and Green, M. R. (2004) U2AF homology motifs: Protein recognition in the RRM world, *Genes Dev. 18*, 1513−1526.
60. Inoue, M., Muto, Y., Sakamoto, H., and Yokoyama, S. (2000) NMR studies on functional structures of the AU-rich element-binding domains of Hu antigen C, *Nucleic Acids Res. 28*, 1743−1750.
61. Gorlach, M., Wittekind, M., Beckman, R. A., Mueller, L., and Dreyfuss, G. (1992) Interaction of the RNA-binding domain of the hnRNP C proteins with RNA, *EMBO J. 11*, 3289−3295.
62. Chi, S. W., Muto, Y., Inoue, M., Kim, I., Sakamoto, H., Shimura, Y., Yokoyama, S., Choi, B. S., and Kim, H. (1999) Chemical shift perturbation studies of the interactions of the second RNA-binding domain of the Drosophila sex-lethal protein with the transformer pre-mRNA polyuridine tract and 3′ splice-site sequences, *Eur. J. Biochem. 260*, 649−660.

BI047450E